

Lattice Boltzmann model for wave propagation

Jianying Zhang, Guangwu Yan,^{*} and Xiubo Shi

College of Mathematics, Jilin University, Changchun 130012, People's Republic of China

(Received 10 October 2008; revised manuscript received 12 May 2009; published 27 August 2009)

A lattice Boltzmann model for two-dimensional wave equation is proposed by using the higher-order moment method. The higher-order moment method is based on the solution of a series of partial differential equations obtained by using multiscale technique and Chapman-Enskog expansion. In order to obtain the lattice Boltzmann model for the wave equation with higher-order accuracy of truncation errors, we removed the second-order dissipation term and the third-order dispersion term by employing the moments up to fourth order. The reversibility in time appears owing to the absence of the second-order dissipation term and the third-order dispersion term. As numerical examples, some classical examples, such as interference, diffraction, and wave passing through a convex lens, are simulated. The numerical results show that this model can be used to simulate wave propagation.

DOI: [10.1103/PhysRevE.80.026706](https://doi.org/10.1103/PhysRevE.80.026706)

PACS number(s): 02.70.-c, 42.25.-p

I. INTRODUCTION

The lattice Boltzmann method (LBM) has been introduced as a new computational tool for the study of fluid dynamics and systems governed by partial differential equations. In the last 20 years, it has been developed as an alternative method for computational fluid dynamics. The LBM originated from a Boolean fluid model known as the lattice gas automata (LGA) [1,2] originally developed to overcome certain drawbacks such as the presence of statistical noise and lack of Galilean invariance of LGA for modeling fluid flow based on kinetic theory [3–7]. Many lattice Boltzmann models have been used to simulate formidable problems such as multiphase flows [8–10], multicomponent flows [11–13], porous media flows [14], flows of suspensions [15,16], compressible flows [17–19], and steady-state flows [20,21]. Additionally, lattice Boltzmann models have been developed to simulate linear and nonlinear partial differential equations such as the Burgers equation [22,23], the Korteweg-de Vries (KdV) equation [24], the Lorenz equations [25], the Schrödinger equation [26–29], the Poisson equation [30,31], and the wave propagation [32–51].

Unlike conventional numerical methods based on macroscopic continuum equation, these LBMs start from mesoscopic kinetic equation, say, the lattice Boltzmann equation, to determine macroscopic fluid flows. Their kinetic nature brings certain advantages over conventional numerical methods, such as their algorithmic simplicity, parallel computation, easy handling of complex boundary conditions, and efficient numerical simulations. Especially their algorithmic simplicity and the flexibility to select equilibrium distribution functions are outstanding advantages.

A number of significantly refined lattice gas and lattice Boltzmann models are proposed for the wave motions. Lattice gas automata for wave propagation [32–36] and acoustic wave [37–39] are given. On the other hand, lattice Boltzmann models for wave motion [40–44], shallow water wave [45], wave propagation in plasmas [46], gravity-capillary in-

ternal wave [47], acoustic wave [48,49], and light wave propagation [50,51] were proposed.

There are two basic problems in the lattice Boltzmann method for wave propagation: (1) how to improve the accuracy of lattice Boltzmann models and (2) how to obtain higher-order accuracy boundary conditions for some complex systems. In this paper, we focus on the first problem.

In order to solve problem (1), we will use a series of partial differential equations in different time scales and higher-order moment method to build wave equation and select suitable forms of the second-order dissipation term and the third-order dispersion term to improve the reversibility of the wave propagation.

In this paper, three open issues on the lattice Boltzmann model are considered. The first issue concerns the approach of how to obtain a higher-order truncation error. If the multiscale technique and the Chapman-Enskog expansion are used, then how many partial differential equations of the series are enough, how many higher-order moments are enough, and what forms of these moments will be. The second issue concerns numerical convergence, numerical stability. What is the trend of the relation between errors and the Knudsen number ε . The third issue concerns how to describe the reversibility in time for wave propagation. The reversibility is regarded as the invariability in form for the wave equation when the time is reversed. If the reversibility in time is used to the lattice Boltzmann model, what is the necessary condition that would be obtained.

In order to simulate a few wave phenomena, such as the interference, diffraction, and propagation of wave passing through a convex lens, we consider linear wave equations,

$$\frac{\partial \rho}{\partial t} + \frac{\partial \rho u_j}{\partial x_j} = 0,$$

$$\frac{\partial \rho u_i}{\partial t} + a^2 \frac{\partial \rho \delta_{ij}}{\partial x_j} = 0, \quad (1)$$

where ρ , \mathbf{u} , and a are the density, the velocity, and the wave speed in a medium, respectively. By simple operating, Eqs. (1) can be returned as the form [52,53,59]

^{*}Corresponding author; yangw@email.jlu.edu.cn

$$\frac{\partial^2 \phi}{\partial t^2} = a^2 \nabla^2 \phi. \quad (2)$$

In the linear wave equation [Eq. (2)], the quantity ϕ expresses density ρ and velocity \mathbf{u} .

Equations (1) are similar to the Euler equations in fluid flows. In fact, the Euler equations will become the above equations if the assumption of small disturbance or small amplitude is employed. The target in the paper is to design a model for Eqs. (1) by using lattice Boltzmann method. However, the strategy selected is not to simulate the wave equation directly by employing the LBM. One reason is that the equation for wave cannot reflect the information of all the physical quantities such as density, velocity of flows, etc. And thus the properties for sound wave but not for wave in another form may be lost, such as the reversibility in time. Another reason is that higher-order moments of the equilibrium distribution function possess simple forms.

This paper is organized as follows, in Sec. II, a lattice Boltzmann model is described. In Sec. III, we give some numerical examples, and Sec. IV gives conclusions.

II. LATTICE BOLTZMANN MODEL

A. Series of partial differential equations in different time scales

The distribution function $f_\alpha(\mathbf{x}, t)$ is defined as one-particle distribution function of unit mass with velocity \mathbf{e}_α , at time t , position \mathbf{x} , here $\alpha=1, \dots, b$ denote moving particles, $\alpha=0$ represents rest particle. The macroscopic variables, mass, and momentum are defined as

$$\rho \equiv \sum_{\alpha} m_{\alpha} f_{\alpha}(\mathbf{x}, t), \quad (3)$$

$$\rho u_j \equiv \sum_{\alpha} m_{\alpha} f_{\alpha}(\mathbf{x}, t) e_{\alpha j}, \quad (4)$$

where m_{α} is the mass of particle. We assume that $m_{\alpha}=m$ for $\alpha \neq 0$ and $m_{\alpha}=m_0$ when $\alpha=0$.

We assume $f_{\alpha}(\mathbf{x}, t)$ possesses the equilibrium distribution function $f_{\alpha}^{eq}(\mathbf{x}, t)$, and it meets the conservation conditions

$$\sum_{\alpha} m_{\alpha} f_{\alpha}^{eq}(\mathbf{x}, t) = \sum_{\alpha} m_{\alpha} f_{\alpha}(\mathbf{x}, t), \quad (5)$$

$$\sum_{\alpha} m_{\alpha} f_{\alpha}^{eq}(\mathbf{x}, t) e_{\alpha j} = \sum_{\alpha} m_{\alpha} f_{\alpha}(\mathbf{x}, t) e_{\alpha j}. \quad (6)$$

The distribution function $f_{\alpha}(\mathbf{x}, t)$ satisfies the lattice Boltzmann equation,

$$f_{\alpha}(\mathbf{x} + \mathbf{e}_{\alpha}, t + 1) - f_{\alpha}(\mathbf{x}, t) = -\frac{1}{\tau} [f_{\alpha}(\mathbf{x}, t) - f_{\alpha}^{eq}(\mathbf{x}, t)], \quad (7)$$

where τ is the single-relaxation time factor.

Using a small parameter ε in numerical simulation, we take it equal to the time step Δt , and $\varepsilon = \Delta x / c$, where Δx is the spatial step and c is the speed of particle. Therefore, ε

can play the role of the Knudsen number [41]. In this case, the lattice Boltzmann equation [Eq. (7)] can be written as

$$f_{\alpha}(\mathbf{x} + \varepsilon \mathbf{e}_{\alpha}, t + \varepsilon) = f_{\alpha}(\mathbf{x}, t) - \frac{1}{\tau} [f_{\alpha}(\mathbf{x}, t) - f_{\alpha}^{eq}(\mathbf{x}, t)]. \quad (8)$$

Taylor expansion is used to Eq. (8), retaining terms up to $O(\varepsilon^7)$; we have

$$f_{\alpha}(\mathbf{x} + \varepsilon \mathbf{e}_{\alpha}, t + \varepsilon) - f_{\alpha}(\mathbf{x}, t) = \sum_{n=1}^6 \frac{\varepsilon^n}{n!} \left(\frac{\partial}{\partial t} + \mathbf{e}_{\alpha} \frac{\partial}{\partial \mathbf{x}} \right)^n f_{\alpha}(\mathbf{x}, t) + O(\varepsilon^7). \quad (9)$$

The Chapman-Enskog expansion [54] is applied to $f_{\alpha}(\mathbf{x}, t)$ under the assumption of small Knudsen number ε ; it is

$$f_{\alpha} = \sum_{n=0}^6 \varepsilon^n f_{\alpha}^{(n)} + O(\varepsilon^7). \quad (10)$$

Introducing t_0, t_1, t_2 as different scale times, we define them as

$$t_i = \varepsilon^i t, \quad i = 0, 1, \dots, 6, \quad (11)$$

and

$$\frac{\partial}{\partial t} = \sum_{n=0}^6 \varepsilon^n \frac{\partial}{\partial t_n} + O(\varepsilon^7). \quad (12)$$

We can obtain a series of partial differential equations as the following:

$$\Delta f_{\alpha}^{(0)} = -\frac{1}{\tau} f_{\alpha}^{(1)}, \quad (13)$$

$$\frac{\partial}{\partial t_1} f_{\alpha}^{(0)} + C_2 \Delta^2 f_{\alpha}^{(0)} = -\frac{1}{\tau} f_{\alpha}^{(2)}, \quad (14)$$

$$C_3 \Delta^3 f_{\alpha}^{(0)} + 2C_2 \Delta \frac{\partial}{\partial t_1} f_{\alpha}^{(0)} + \frac{\partial}{\partial t_2} f_{\alpha}^{(0)} = -\frac{1}{\tau} f_{\alpha}^{(3)}, \quad (15)$$

$$C_4 \Delta^4 f_{\alpha}^{(0)} + 3C_3 \Delta^2 \frac{\partial}{\partial t_1} f_{\alpha}^{(0)} + 2C_2 \Delta \frac{\partial}{\partial t_2} f_{\alpha}^{(0)} + \frac{\partial}{\partial t_3} f_{\alpha}^{(0)} + C_2 \frac{\partial^2}{\partial t_1^2} f_{\alpha}^{(0)} = -\frac{1}{\tau} f_{\alpha}^{(4)}, \quad (16)$$

$$C_5 \Delta^5 f_{\alpha}^{(0)} + 4C_4 \Delta^3 \frac{\partial}{\partial t_1} f_{\alpha}^{(0)} + 3C_3 \Delta^2 \frac{\partial}{\partial t_2} f_{\alpha}^{(0)} + 2C_2 \Delta \frac{\partial}{\partial t_3} f_{\alpha}^{(0)} + \frac{\partial}{\partial t_4} f_{\alpha}^{(0)} + 3C_3 \Delta \frac{\partial^2}{\partial t_1^2} f_{\alpha}^{(0)} + 2C_2 \frac{\partial^2}{\partial t_1 \partial t_2} f_{\alpha}^{(0)} = -\frac{1}{\tau} f_{\alpha}^{(5)}, \quad (17)$$

$$\begin{aligned}
& C_6 \Delta^6 f_\alpha^{(0)} + 5C_5 \Delta^4 \frac{\partial}{\partial t_1} f_\alpha^{(0)} + 4C_4 \Delta^3 \frac{\partial}{\partial t_2} f_\alpha^{(0)} + 3C_3 \Delta^2 \frac{\partial}{\partial t_3} f_\alpha^{(0)} \\
& + 2C_2 \Delta \frac{\partial}{\partial t_4} f_\alpha^{(0)} + \frac{\partial}{\partial t_5} f_\alpha^{(0)} + 6C_4 \Delta^2 \frac{\partial^2}{\partial t_1^2} f_\alpha^{(0)} \\
& + 6C_3 \Delta \frac{\partial^2}{\partial t_1 \partial t_2} f_\alpha^{(0)} + 2C_2 \frac{\partial^2}{\partial t_1 \partial t_3} f_\alpha^{(0)} + C_3 \frac{\partial^3}{\partial t_1^3} f_\alpha^{(0)} \\
& + C_2 \frac{\partial^2}{\partial t_2^2} f_\alpha^{(0)} = -\frac{1}{\tau} f_\alpha^{(6)}, \tag{18}
\end{aligned}$$

where $f_\alpha^{(0)} \equiv f_\alpha^{eq}$ and the partial differential operator $\Delta \equiv \partial / \partial t_0 + \mathbf{e}_\alpha \cdot (\partial / \partial \mathbf{x})$.

Equations (13)–(18) are so-called series of partial differential equations in different time scales. It is suitable for one-dimensional, two-dimensional, and three-dimensional cases. Five polynomials of the relaxation time factor τ in Eqs. (13)–(18) are found; they are the following:

$$C_1 = 1, \tag{19}$$

$$C_2 = \frac{1}{2} - \tau, \tag{20}$$

$$C_3 = \tau^2 - \tau + \frac{1}{6} = C_2^2 - \frac{1}{12}, \tag{21}$$

$$C_4 = -\tau^3 + \frac{3}{2}\tau^2 - \frac{7}{12}\tau + \frac{1}{24} = C_2^3 - \frac{1}{6}C_2, \tag{22}$$

$$C_5 = \tau^4 - 2\tau^3 + \frac{5}{4}\tau^2 - \frac{1}{4}\tau + \frac{1}{120} = C_2^4 - \frac{1}{4}C_2^2 + \frac{1}{120}, \tag{23}$$

$$C_6 = -\tau^5 + \frac{5}{2}\tau^4 - \frac{13}{6}\tau^3 + \frac{3}{4}\tau^2 - \frac{31}{360}\tau + \frac{1}{720} = C_2^5 - \frac{1}{3}C_2^3 + \frac{17}{720}C_2. \tag{24}$$

Equations (19)–(24) are the first six Bernoulli polynomials, which are in full agreement with the results in the literature [55]. They can be used to indicate coefficients of the dispersion term and the dissipation term to the modified macroscopic equation.

B. Moments of the equilibrium distribution function

Combining Eqs. (3)–(6), we have

$$\sum_\alpha f_\alpha^{(n)}(\mathbf{x}, t) m_\alpha = 0, \quad \sum_\alpha f_\alpha^{(n)}(\mathbf{x}, t) m_\alpha e_{\alpha j} = 0, \quad n \geq 1. \tag{25}$$

Other moments of the equilibrium distribution function are denoted as the following:

$$\sum_\alpha m_\alpha f_\alpha^{(0)}(\mathbf{x}, t) e_{\alpha i} e_{\alpha j} \equiv \pi_{ij}^0(\mathbf{x}, t), \tag{26}$$

$$\sum_\alpha m_\alpha f_\alpha^{(0)}(\mathbf{x}, t) e_{\alpha i} e_{\alpha j} e_{\alpha k} \equiv P_{ijk}^0(\mathbf{x}, t), \tag{27}$$

$$\sum_\alpha m_\alpha f_\alpha^{(0)}(\mathbf{x}, t) e_{\alpha i} e_{\alpha j} e_{\alpha k} e_{\alpha m} \equiv Q_{ijklm}^0(\mathbf{x}, t). \tag{28}$$

Multiplying m_α and summing Eq. (13) with respect to α , we obtain

$$\frac{\partial \rho}{\partial t_0} + \frac{\partial \rho u_j}{\partial x_j} = 0. \tag{29}$$

Multiplying m_α and $e_{\alpha i}$ and summing Eq. (13) over α , we have

$$\frac{\partial \rho u_i}{\partial t_0} + \frac{\partial \pi_{ij}^0}{\partial x_j} = 0. \tag{30}$$

If we select

$$\pi_{ij}^0 = \sum_\alpha m_\alpha f_\alpha^{(0)} e_{\alpha i} e_{\alpha j} = \lambda m \rho \delta_{ij}, \tag{31}$$

we have the wave equations in time scale t_0 ,

$$\frac{\partial \rho}{\partial t_0} + \frac{\partial \rho u_j}{\partial x_j} = 0, \tag{32}$$

$$\frac{\partial \rho u_i}{\partial t_0} + \lambda m \frac{\partial \rho \delta_{ij}}{\partial x_j} = 0, \tag{33}$$

where λ is a parameter to be determined by the wave speed. Operating (13)+(14) ε +(15) ε^2 +(16) ε^3 , multiplying m_α , and summing over α , we have

$$\frac{\partial \rho}{\partial t} + \frac{\partial \rho u_j}{\partial x_j} + E_1 + E_2 + E_3 = O(\varepsilon^4). \tag{34}$$

Making (13)+(14) ε +(15) ε^2 +(16) ε^3 , multiplying m_α and $e_{\alpha i}$, and summing over α , we have

$$\frac{\partial \rho u_i}{\partial t} + \frac{\partial \pi_{ij}^0}{\partial x_j} + R_1 + R_2 + R_3 = O(\varepsilon^4). \tag{35}$$

In Eqs. (34) and (35),

$$E_1 = \varepsilon \sum_\alpha m_\alpha C_2 \Delta^2 f_\alpha^{(0)}, \tag{36}$$

$$E_2 = \varepsilon^2 \sum_\alpha m_\alpha \left(2C_2 \Delta \frac{\partial}{\partial t_1} f_\alpha^{(0)} + C_3 \Delta^3 f_\alpha^{(0)} \right), \tag{37}$$

$$\begin{aligned}
E_3 = \varepsilon^3 \sum_\alpha m_\alpha \left(C_4 \Delta^4 f_\alpha^{(0)} + 3C_3 \Delta^2 \frac{\partial}{\partial t_1} f_\alpha^{(0)} \right. \\
\left. + 2C_2 \Delta \frac{\partial}{\partial t_2} f_\alpha^{(0)} + C_2 \frac{\partial^2}{\partial t_1^2} f_\alpha^{(0)} \right), \tag{38}
\end{aligned}$$

$$R_1 = \varepsilon \sum_\alpha m_\alpha e_{\alpha i} C_2 \Delta^2 f_\alpha^{(0)}, \tag{39}$$

$$R_2 = \varepsilon^2 \sum_\alpha m_\alpha \left(2C_2 \Delta \frac{\partial}{\partial t_1} f_\alpha^{(0)} + C_3 \Delta^3 f_\alpha^{(0)} \right) e_{\alpha i}, \tag{40}$$

$$\begin{aligned}
 R_3 = \varepsilon^3 \sum_{\alpha} m_{\alpha} & \left(C_4 \Delta^4 f_{\alpha}^{(0)} + 3C_3 \Delta^2 \frac{\partial}{\partial t_1} f_{\alpha}^{(0)} \right. \\
 & \left. + 2C_2 \Delta \frac{\partial}{\partial t_2} f_{\alpha}^{(0)} + C_2 \frac{\partial^2}{\partial t_1^2} f_{\alpha}^{(0)} \right) e_{\alpha i}. \quad (41)
 \end{aligned}$$

According to Eqs. (34) and (35), the modified wave equation for Eq. (2) is

$$\begin{aligned}
 \frac{\partial^2 \rho}{\partial t^2} - \frac{\partial^2 \pi_{ij}^0}{\partial x_i \partial x_j} + \frac{\partial E_1}{\partial t} - \frac{\partial R_1}{\partial x_i} + \frac{\partial E_2}{\partial t} - \frac{\partial R_2}{\partial x_i} + \frac{\partial E_3}{\partial t} - \frac{\partial R_3}{\partial x_i} \\
 = O(\varepsilon^4). \quad (42)
 \end{aligned}$$

Obviously, the second-order dissipation term and the third-order dispersion term of the modified macroscopic equation [Eq. (42)] are

$$T_2 = \frac{\partial E_1}{\partial t} - \frac{\partial R_1}{\partial x_i}, \quad (43)$$

$$T_3 = \frac{\partial E_2}{\partial t} - \frac{\partial R_2}{\partial x_i}. \quad (44)$$

In order to remove the dissipation term and the dispersion term, other two moments are used,

$$P_{ijk}^0 = \frac{1}{3} \lambda m \rho (u_i \delta_{jk} + u_j \delta_{ik} + u_k \delta_{ij}), \quad (45)$$

$$Q_{ijkl}^0 = \frac{1}{3} \lambda^2 m^2 \rho (\delta_{ij} \delta_{kl} + \delta_{ik} \delta_{jl} + \delta_{il} \delta_{jk}). \quad (46)$$

The detailed derivations of error terms T_2 and T_3 are given in Appendix. They are

$$\begin{aligned}
 T_2 = \frac{\partial E_1}{\partial t} - \frac{\partial R_1}{\partial x_i} = -\frac{\partial R_1}{\partial x_i} = -\frac{\partial}{\partial x_i} \varepsilon C_2 \frac{\partial}{\partial x_k} \left(\frac{\partial \pi_{ki}^0}{\partial t_0} + \frac{\partial P_{ijk}^0}{\partial x_j} \right) = 0, \quad (47)
 \end{aligned}$$

$$\begin{aligned}
 T_3 = \frac{\partial E_2}{\partial t} - \frac{\partial R_2}{\partial x_i} = -\frac{\partial R_2}{\partial x_i} \\
 = -\varepsilon^2 C_3 \frac{\partial}{\partial x_i} \left\{ \frac{\partial}{\partial x_k} \left[\frac{\partial}{\partial x_m} \left(\frac{\partial P_{ikm}^0}{\partial t_0} + \frac{\partial Q_{ijkm}^0}{\partial x_j} \right) \right] \right\} \\
 = 0. \quad (48)
 \end{aligned}$$

Based on $\pi_{ij}^0 = \lambda m \rho \delta_{ij}$, Eq. (42) becomes

$$\frac{\partial^2 \rho}{\partial t^2} = \lambda m \frac{\partial^2 \rho}{\partial x_j \partial x_j} + O(\varepsilon^3). \quad (49)$$

Therefore, we have obtained wave equation with third-order accuracy of the truncation errors.

C. Equilibrium distribution function

Let us consider a two-layer b -side regular polygon lattice with $2b$ links that connect the center site to $2b$ neighbor nodes. We assume that the particles moving along the link with velocity \mathbf{e}_{α} are divided into three kinds, $|\mathbf{e}_{\alpha}| = c$, $|\mathbf{e}_{\alpha}| = 2c$, and $|\mathbf{e}_{\alpha}| = 0$, where c is the speed of particles in a direc-

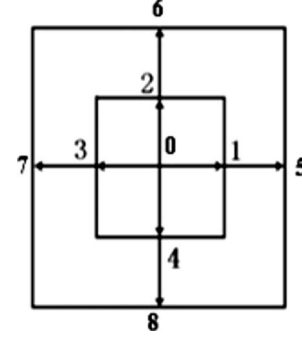


FIG. 1. Two-dimensional three-speed 9 bit lattice, $b=4$.

tion of small b -side regular polygon (see Fig. 1). So it is actually a $2b+1$ bit model with three speeds, 0, c , and $2c$, i.e.,

$$|\mathbf{e}_{\alpha}| = \begin{cases} c, & \alpha = 1, \dots, b \\ 2c, & \alpha = b+1, \dots, 2b \\ 0, & \alpha = 0. \end{cases} \quad (50)$$

Assuming the equilibrium distribution function has the form

$$f_{\alpha}^{(0)} = A_0 \rho + A_2 e_{\alpha j} \rho u_j, \quad \alpha = 1, \dots, b,$$

$$f_{\alpha}^{(0)} = B_0 \rho + B_2 e_{\alpha j} \rho u_j, \quad \alpha = b+1, \dots, 2b,$$

$$f_0^{(0)} = D_0 \rho, \quad (51)$$

we can find the parameters in Eq. (51) by using Eqs. (5), (6), (31), (45), and (46); they are

$$A_0 = \frac{1}{12bc^4} \left[16\lambda Dc^2 - \frac{4}{3} D(D+2)\lambda^2 m \right], \quad (52)$$

$$B_0 = \frac{1}{12bc^4} \left[-\lambda Dc^2 + \frac{1}{3} D(D+2)\lambda^2 m \right], \quad (53)$$

$$D_0 = \frac{1}{m_0} - \frac{m}{m_0} \frac{1}{12c^4} [15\lambda Dc^2 - D(D+2)\lambda^2 m], \quad (54)$$

$$A_2 = \frac{1}{12bc^4 m} \left[16Dc^2 - \frac{4}{3} D(D+2)\lambda m \right], \quad (55)$$

$$B_2 = \frac{1}{12bc^4 m} \left[-Dc^2 + \frac{1}{3} D(D+2)\lambda m \right]. \quad (56)$$

In Eqs. (52)–(56), D ($=2$) is the spatial dimension.

D. Analysis of error term and Hirt's heuristic stability conditions

The error term of Eq. (42) is

$$T_4 = \frac{\partial E_3}{\partial t} - \frac{\partial R_3}{\partial x_i} = -\varepsilon^3 C_4 \frac{\partial}{\partial x_i} \frac{\partial}{\partial x_k} \frac{\partial}{\partial x_m} \frac{\partial}{\partial x_j} \frac{\partial}{\partial x_l} \times \left[-\frac{1}{3} \lambda^2 m^2 \Delta_{ijklm} \rho u_l + R_{ijklm}^0 \right], \quad (57)$$

where $\Delta_{ijklm} = \delta_{ij} \delta_{km} + \delta_{ik} \delta_{jm} + \delta_{im} \delta_{jk}$. In Eq. (57), $R_{ijklm}^0 = \sum_{\alpha} m_{\alpha} f_{\alpha}^0 e_{\alpha i} e_{\alpha j} e_{\alpha k} e_{\alpha l} e_{\alpha m}$. According to the expression of equilibrium distribution function, we have

$$T_4 = \frac{\partial E_3}{\partial t} - \frac{\partial R_3}{\partial x_i} = -\varepsilon^3 C_4 (-\lambda^2 m^2 + 9\beta) \nabla^4 (\nabla \cdot \rho \mathbf{u}), \quad (58)$$

where $\nabla^4 = \partial^4 / \partial x_i \partial x_j \partial x_k \partial x_l$, and $\beta = [c^2 / D(D+2)(D+4)] \times [-4Dc^2 + \frac{5}{3}D(D+2)\lambda m]$. The detailed derivation of error term T_4 is given in Appendix.

In Eq. (42), the fourth-order dissipation term is $T_4 = -\varepsilon^3 C_4 (-\lambda^2 m^2 + 9\beta) \nabla^4 (\nabla \cdot \rho \mathbf{u})$. According to the Hirt's heuristic stability theory [56,57], the coefficient $\varepsilon^3 C_4 (-\lambda^2 m^2 + 9\beta) > 0$ is the necessary stability condition. Therefore, the stability of the lattice Boltzmann equation [Eq. (7)] is controlled by the condition $\varepsilon^3 C_4 (-\lambda^2 m^2 + 9\beta) > 0$.

E. Wave speed and refraction ratio

According to Eq. (49), we obtain the wave speed as

$$c_s = \sqrt{\lambda m}. \quad (59)$$

Let us introduce the refraction ratio n . It is defined as a ratio of the free propagation speed $c/\sqrt{2}$ to the wave speed c_s ; therefore

$$n^2 = \frac{c^2}{2c_s^2}. \quad (60)$$

According to Ref. [40], we select

$$\frac{m_0}{m} = 2\sqrt{n^2 - 1}. \quad (61)$$

F. Reversibility in time for wave propagation

The reversibility is regarded as the invariability in form for the wave equation when the time is reversed. We replace t by $-t$; Eq. (42) becomes

$$\frac{\partial^2 \rho}{\partial t^2} - \frac{\partial^2 \pi_{ij}^0}{\partial x_i \partial x_j} - \frac{\partial E_1}{\partial t} - \frac{\partial R_1}{\partial x_i} - \frac{\partial E_2}{\partial t} - \frac{\partial R_2}{\partial x_i} - \frac{\partial E_3}{\partial t} - \frac{\partial R_3}{\partial x_i} = O(\varepsilon^4). \quad (62)$$

The error terms are

$$T'_2 = -\frac{\partial E_1}{\partial t} - \frac{\partial R_1}{\partial x_i}, \quad (63)$$

$$T'_3 = -\frac{\partial E_2}{\partial t} - \frac{\partial R_2}{\partial x_i}, \quad (64)$$

$$T'_4 = -\frac{\partial E_3}{\partial t} - \frac{\partial R_3}{\partial x_i}. \quad (65)$$

Based on Eqs. (A1), (A5), and (A12) in Appendix, we obtain

$$T'_2 = -\frac{\partial R_1}{\partial x_i} = T_2 = 0, \quad (66)$$

$$T'_3 = -\frac{\partial R_2}{\partial x_i} = T_3 = 0, \quad (67)$$

$$T'_4 = -\frac{\partial R_3}{\partial x_i} = T_4. \quad (68)$$

Thus, Eq. (62) becomes

$$\frac{\partial^2 \rho}{\partial t^2} = \lambda m \frac{\partial^2 \rho}{\partial x_j \partial x_j} + O(\varepsilon^3). \quad (69)$$

Equation (49) and its reversal equation [Eq. (69)] have the same form when the truncation errors $O(\varepsilon^3)$ are ignored. Therefore, the higher-order moments [Eqs. (31), (45), and (46)] are reasons that the lattice Boltzmann model possesses the reversibility in time and the third-order accuracy of truncation errors.

III. NUMERICAL EXAMPLES

In this section, we choose a series of numerical experiments to test this method for the two-dimensional model.

A. Two-dimensional wave

Consider the two-dimensional wave equation,

$$\frac{\partial^2 \psi}{\partial t^2} = C_s^2 \nabla^2 \psi, \quad 0 < x < 1, \quad 0 < y < 1, \quad t > 0. \quad (70a)$$

Its initial condition and boundary conditions are

$$\psi(x, y, 0) = \sin \pi x \sin \pi y, \quad (70b)$$

$$\psi(0, y, t) = \psi(1, y, t) = 0, \quad (70c)$$

$$\psi(x, 0, t) = \psi(x, 1, t) = 0, \quad (70d)$$

$$\frac{\partial \psi(x, y, 0)}{\partial t} = 0. \quad (70e)$$

The analytical solution is

$$\psi(x, y, t) = \sin(\pi x) \sin(\pi y) \cos(\sqrt{2} \pi C_s t). \quad (71)$$

In Fig. 2, the comparison of exact solution and LBM result is given. Figure 2(a) is the exact solution. Figure 2(b) is the LBM result. In addition, in order to see the comparison in

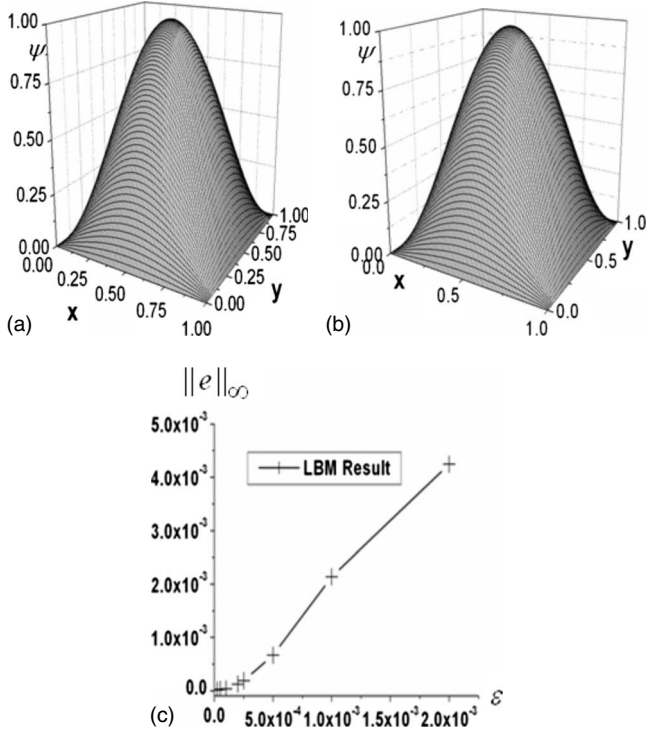


FIG. 2. Comparison of exact solution and the LBM result of two-dimensional wave equation. (a) Exact solution and (b) LBM result of wave equation. (c) is the curve of the infinite norm of the relative error $\|e\|_\infty$ versus the Knudsen number ε . Parameters are $c = 3.0$, lattice size 100×100 for (a) and (b), $\tau = 0.5$, $C_s = 0.01$, and $t = 0.6$.

detail, we define the relative error as $e = |(\psi^N - \psi^E) / \psi^E|$ and plot the curve of the infinite norm of the relative error $\|e\|_\infty$ versus the Knudsen number ε to the example, at $x = 0.6$, $t = 0.6$ [see Fig. 2(c)], where ψ^N and ψ^E are the LBM result and exact solution, respectively. If $c = 3.0$ is fixed, the spatial step $\Delta x = c\varepsilon$ is proportional to the Knudsen number ε . Thus, Fig. 2(c) shows the relation between the truncation error and the spatial step. It provides a qualitative trend of the numerical order of convergence. We can find that the LBM result is in close agreement with exact solution.

B. Simulations for the interference, diffraction, Young’s experiment, and go-through convex lens

Let us consider a rectangle region. The boundary conditions of the variables are divided into two kinds of cases: (1) left, right, upper, and bottom boundary and (2) solid wall boundary. For case (1), the Neumann boundary conditions are employed; for case (2) we use the Dirichlet boundary condition as velocity $u_j = 0$ and density $\rho = 0$.

In the numerical simulations, the region is adjusted to $[0, 2] \times [0, 1]$. We select the square lattice, and the lattice size is 200×100 , thus $\Delta x = \Delta y = 0.01$.

1. Interference of two point sources

The experiment is done at the conditions of the unit mass of particle selected as $m = \frac{3}{16}$ and the refraction ratio set as

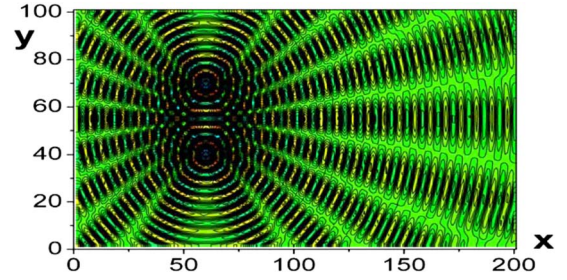


FIG. 3. (Color online) The interference pattern of two point sources at time $t = 300\Delta t$ by using lattice Boltzmann method. The coordinates are denoted by the numbers of cells in x and y directions. Parameters are $c = 3.0$, lattice size 200×100 , $\tau = 0.5$, $n = 1.0$, and $m = \frac{3}{16}$. The number of color levels is 30.

$n = 1.0$. And so are the remains except for the example of lens $n = 1.8$. Two point sources are located at $(60\Delta x, 40\Delta y)$ and $(60\Delta x, 70\Delta y)$. They are

$$\rho(60\Delta x, 40\Delta y, t) = \rho(60\Delta x, 70\Delta y, t) = \sin(\omega t). \quad (72)$$

In Eq. (72), $\omega = 2\pi/T$, where $T = 10\Delta t$ is the period, Δt is the time step. The boundary conditions are Neumann conditions, i.e.,

$$\begin{aligned} \frac{\partial F(0, y, t)}{\partial x} &= 0, & \frac{\partial F(2, y, t)}{\partial x} &= 0, \\ \frac{\partial F(x, 0, t)}{\partial y} &= 0, & \frac{\partial F(x, 1, t)}{\partial y} &= 0, \end{aligned}$$

where F denotes small perturbation variables: density ρ , pressure p , and flow velocity components in x and y directions, u and v , respectively. In Fig. 3, we plot the contours of ρ at $t = 300\Delta t$ by using lattice Boltzmann method. It is the interference pattern of two point sources.

2. Diffraction of single hole

At 80 cells away from the left boundary a baffle plate with a hole of five cells is inserted. In the test, we use a point source at $(30\Delta x, 50\Delta y)$. It has the same vibration as Eq. (72). We can observe that wave can go through the hole into the right region and form the pattern of diffraction (see Fig. 4).

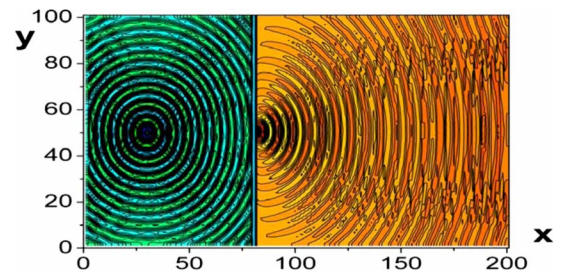


FIG. 4. (Color online) The diffraction pattern of single hole at time $t = 500\Delta t$ by using lattice Boltzmann method. The coordinates are denoted by the numbers of cells in x and y directions. Parameters are $c = 3.0$, lattice size 200×100 , $\tau = 0.5$, $n = 1.0$, and $m = \frac{3}{16}$. The number of color levels is 50.

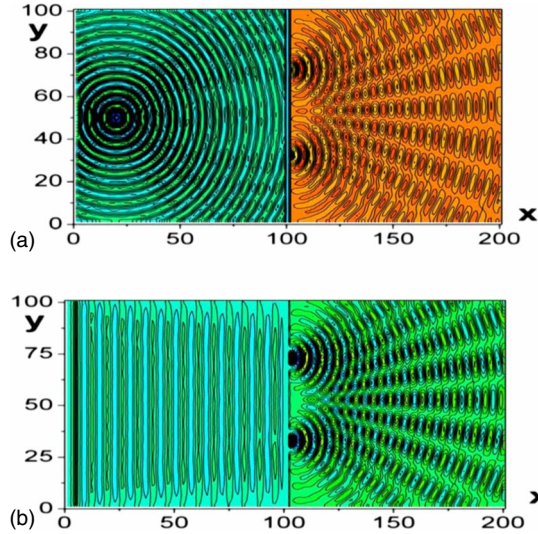


FIG. 5. (Color online) (a) The interference pattern of the double slit by using lattice Boltzmann method. (b) The interference pattern of the LBM result with a point source at time $t=3000\Delta t$. The interference pattern of the LBM result with the line segment source at time $t=1000\Delta t$. The coordinates are denoted by the numbers of cells in x and y directions. Parameters are $c=3.0$, lattice size 200×100 , $\tau=0.5$, $n=1.0$, and $m=\frac{3}{16}$. The number of color levels is 50.

3. Interference of the double-slit

In this test, at 100 cells away from the left boundary a baffle plate with two holes of six cells is inserted. The center of holes are $(100\Delta x, 30\Delta y)$ and $(100\Delta x, 70\Delta y)$. We use two kinds of wave sources to observe the phenomenon of interference: a point source and a line segment source. The point source is located at $(20\Delta x, 50\Delta y)$. The line segment source is located at $x=5\Delta x$ from $y=0$ to $y=100\Delta y$. They have the same vibration as Eq. (72). In these two circumstances, the interference appears (see Fig. 5). Figure 5(a) is the interference of the double slit with a point source. Figure 5(b) is the interference of the double slit with the line segment source. The figure demonstrates that the wave cannot only go through the two holes into the right region, but then the similar interference phenomena appear.

4. Young's experiment

In this simulation, two baffle plates are inserted. The first baffle plate is located at $x=60\Delta x$ with a hole of six cells. The center of the hole is $(60\Delta x, 48\Delta y)$. The second baffle plate is located at $x=120\Delta x$ with two holes of six cells. The centers of the holes are $(120\Delta x, 43\Delta y)$ and $(120\Delta x, 68\Delta y)$. We employ a point source located at $(20\Delta x, 50\Delta y)$ with the same vibration as Eq. (72). The result of lattice Boltzmann simulation is shown in Fig. 6. From this pattern, we can see that the wave can go through the holes of two baffle plates and into the middle and the right regions. Though the wave intensity is weakened as it goes through the holes, it can also be regarded as a source to produce the phenomena of diffraction and interference.

5. Light go through a convex lens

As to the results of light go through a convex lens, we simulate two cases: (1) the light starting from a point source

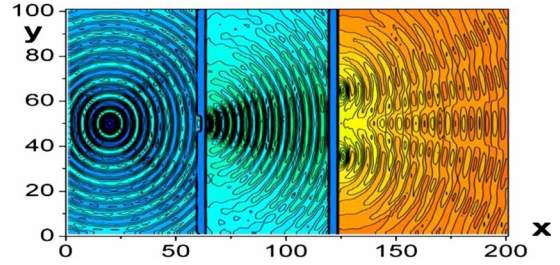


FIG. 6. (Color online) The pattern of the Young's experiment by using lattice Boltzmann method with a point source at time $t=2000\Delta t$. The coordinates are denoted by the numbers of cells in x and y directions. Parameters are $c=3.0$, lattice size 200×100 , $\tau=0.5$, $n=1.0$, and $m=\frac{3}{16}$. The number of color levels is 85.

goes through a convex lens and becomes plane light. The convex lens is located at $x=50\Delta x$. The point source is located at $(65\Delta x, 50\Delta y)$. The result of LBM is given in Fig. 7(a). (2) Plane light goes through a convex lens and focuses on the focus. The convex lens is located at $x=100\Delta x$. The line segment source is located at $x=5\Delta x$ from $y=0$ to $y=100\Delta y$. The result of LBM is given in Fig. 7(b). We can find the focus of the convex lens.

C. Computation of truncation error of the LBM

In order to compute the truncation error of the LBM, we employ the numerical results of the alternating direction implicit (ADI) Fairweather-Mitchell scheme [58] as exact numerical results. The absolute error is defined as $R=(\rho_N - \rho_A)$, where ρ_N, ρ_A are the density of the LBM result and that of the ADI Fairweather-Mitchell scheme result, respec-

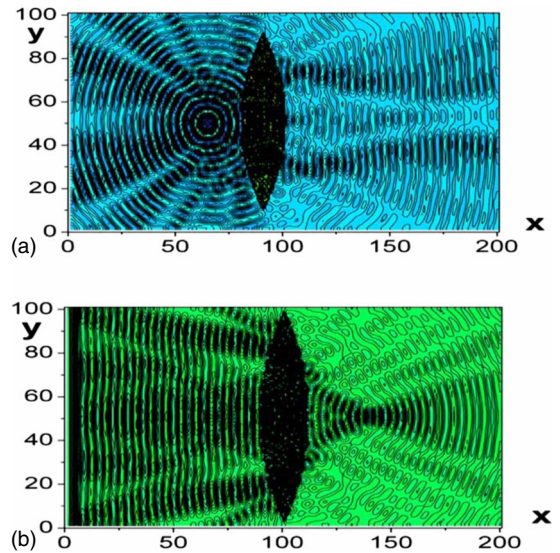


FIG. 7. (Color online) (a) The pattern of light go through a convex lens by using lattice Boltzmann method. (b) Point light source goes through the convex lens at time $t=2000\Delta t$. Plane light source goes through the convex lens at time $t=2000\Delta t$. The coordinates are denoted by the numbers of cells in x and y directions. Parameters are $c=3.0$, lattice size 200×100 , $\tau=0.5$, the refraction ratio $n=1.8$, and $m=\frac{3}{16}$. The number of color levels is 85.

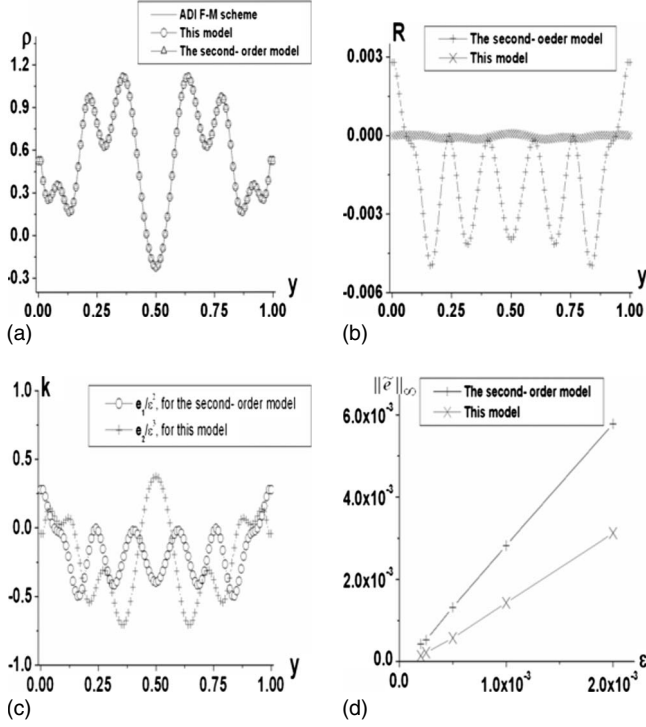


FIG. 8. (a) is the comparison between density by the ADI Fairweather-Mitchell scheme and the LBM result, the result by the second-order model in Ref. [41]. (b) is the curves of the absolute errors of the LBM model and the second-order model. (c) is the curves of the coefficient k versus vertical position y at $x=180\Delta x$. (d) is the curves of the infinite norm of the absolute error $\|\bar{e}\|_\infty$ versus the Knudsen number ε with a fixed $c=3.0$ at $x=0.18$, $0 < y < 1$. Parameters are $c=3.0$, lattice size 200×100 for (a)–(c), $\tau=0.5$, time $t=1000\Delta t$, $n=1.0$, and $m=\frac{3}{16}$.

tively. Let us consider the interference of the double slit of the two-dimensional wave propagation in the region $[0, 2] \times [0, 1]$. The lattice size is set as 200×100 . In this test, at 100 cells away from the left boundary a baffle plate with two holes of six cells is inserted. The centers of holes are located at $(100\Delta x, 30\Delta y)$ and $(100\Delta x, 70\Delta y)$. The line segment source is located at $x=5\Delta x$ from $y=0$ to $y=100\Delta y$, with the vibration $\sin(\omega t)$. The interference pattern of the LBM result at time $t=1000\Delta t$ has been plotted in Fig. 5(b).

In Fig. 8(a), the comparison of the density by the ADI Fairweather-Mitchell scheme, the LBM result in this paper, and the result by the second-order model in Ref. [41] is given. In this figure, the region is $x=180\Delta x$, $0 < y < 100\Delta y$, the solid line is the result of the ADI Fairweather-Mitchell scheme, and circles and triangle are the LBM result and the second-order model in Ref. [41], respectively. We find that the LBM in this paper is the same as the second-order model. Nevertheless, by further comparison, we find that absolute errors R are different in Fig. 8(b). The absolute errors of the second-order model are in the scope of $(-6.0 \times 10^{-3}, 6.0 \times 10^{-3})$, but the absolute errors of this model are in an even smaller scope.

In order to examine the order of the truncation error for the model, we define the coefficient k as the proportion of the truncation error to the order of the model in the Knudsen

number ε . That is, $k=e_1/\varepsilon^2$ for the second-order model and $k=e_2/\varepsilon^3$ for the third-order model, where e_1 and e_2 are the truncation errors of the second-order model and the third-order model, respectively. It is clear that truncation error is $O(\varepsilon^3)$ for this model when k is a finite number. In Fig. 8(c), we plot curves of the coefficient versus vertical position y at $x=180\Delta x$. We find that the coefficient k of this model is within the scope of $(-1.0, 1.0)$. The result shows the model possesses the third-order accuracy of truncation errors. At the same time, we find that the second-order model possesses the second-order accuracy of truncation errors.

We also plot the curves of the infinite norm of the absolute error $\|\bar{e}\|_\infty$ versus the Knudsen number ε with a fixed $c=3.0$ at $x=0.18$, $0 < y < 1$ [see Fig. 8(d)]. The absolute error is defined as $\bar{e}=|\rho_N(0.18, y)-\rho_A(0.18, y)|$, where ρ_N is the density of the LBM result and ρ_A is the numerical result of the ADI Fairweather-Mitchell scheme. Thus, this figure shows the relation between the truncation error and the lattice size and provides a qualitative trend of the numerical order of convergence. From Fig. 8(d), we can see that the LBM results agree well with ADI Fairweather-Mitchell scheme solution.

D. Reversibility in time

In order to compute the reversibility in time, we introduce two kinds of procedures, direct evolution and inverse evolution. For convenience, the lattice Boltzmann equation [Eq. (7)] can be rewritten as the following form:

$$f_\alpha(\mathbf{x}, t) = f_\alpha(\mathbf{x} - \Delta t \mathbf{e}_\alpha, t - \Delta t) - \frac{1}{\tau} [f_\alpha(\mathbf{x} - \Delta t \mathbf{e}_\alpha, t - \Delta t) - f_\alpha^{eq}(\mathbf{x} - \Delta t \mathbf{e}_\alpha, t - \Delta t)]. \quad (73)$$

Equation (73) is regarded as the direct evolution. By using $-\Delta t$ instead of Δt , the inverse evolution lattice Boltzmann equation is obtained,

$$f_\alpha(\mathbf{x}, t - \Delta t) = f_\alpha(\mathbf{x} + \Delta t \mathbf{e}_\alpha, t) - \frac{1}{\tau} [f_\alpha(\mathbf{x} + \Delta t \mathbf{e}_\alpha, t) - f_\alpha^{eq}(\mathbf{x} + \Delta t \mathbf{e}_\alpha, t)]. \quad (74)$$

The difference of direct evolution [Eq. (7)] and inverse evolution [Eq. (74)] is the flux procedure in computation. Therefore, we use two kinds of flux procedures, direct flux and inverse flux; they are $f_\alpha(\mathbf{x}, t + \Delta t) \leftarrow f_\alpha(\mathbf{x} - \Delta t \mathbf{e}_\alpha, t + \Delta t)$ and $f_\alpha(\mathbf{x}, t - \Delta t) \leftarrow f_\alpha(\mathbf{x} + \Delta t \mathbf{e}_\alpha, t - \Delta t)$, respectively.

Consider a rectangle region $[0, 200\Delta x] \times [0, 100\Delta y]$, where $\Delta x = \Delta y = 0.01$. The line segment source is located at $x=5\Delta x$ from $y=0$ to $y=100\Delta y$ with $\sin(\omega t)$. The simulation is divided into two procedures: (1) direct evolution from $t=0$ to $t=200\Delta t$ and (2) inverse evolution without the line segment source from the state of the direct evolution at $t=200\Delta t$ to $t=0$. We give attention to two kinds of errors, the residue errors and the recovery errors; they are $e=|\rho_D - \rho_I|$ and $R=|S_D - S_I|$, where ρ_D , ρ_I are the densities of the direct evolution and inverse evolution at the same moment,

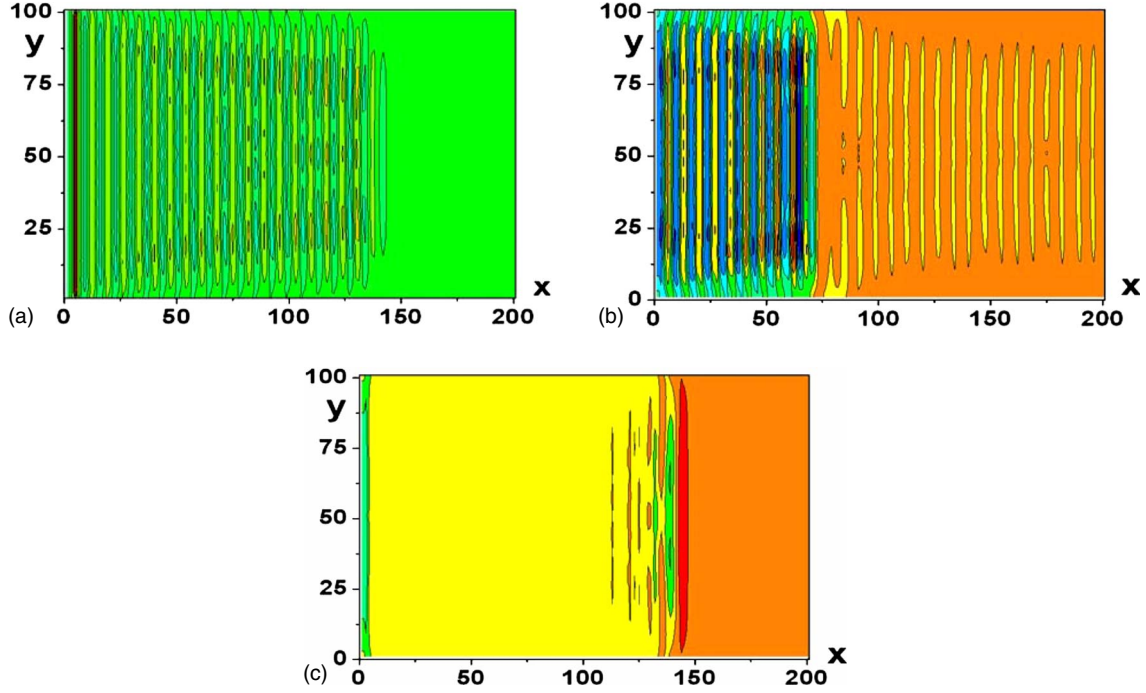


FIG. 9. (Color online) (a) The pattern of density for the direct evolution from a static velocity field to $t=200\Delta t$. (b) The pattern of density for the inverse evolution without the line segment source from the state of the direct evolution at $t=200\Delta t$ to $t=100\Delta t$. (c) The pattern of density for the inverse evolution without the line segment source from the state of the direct evolution at $t=200\Delta t$ to $t=0$. The coordinates are denoted by the numbers of cells in x and y directions. Parameters are $c=3.0$, lattice size 200×100 , $\tau=0.5$, $n=1.0$, and $m=\frac{3}{16}$. The number of color levels is 10.

respectively, and S_D , S_I are the densities of the direct evolution and inverse evolution near the source at the same moment, respectively.

In Fig. 9(a), we plot the pattern of density for the direct evolution from a static velocity field to $t=200\Delta t$. The wave front is within $x < 150\Delta x$. Figure 9(b) is the pattern of density for the inverse evolution without the line segment source from the state of the direct evolution at $t=200\Delta t$ to $t=100\Delta t$. After the wave inversion, the phenomena of the wave front moving back away and the disturbance waves in the residue region are found. Figure 9(c) is the pattern of density for the inverse evolution without the line segment source from the state of the direct evolution at $t=200\Delta t$ to $t=0$. In the case of Fig. 9(c), the waves have vanished, but the disturbance waves are still remaining.

We also plot the curve of the residue errors $e=|\rho_D-\rho_I|$ versus X axis with a fixed $y=50\Delta y$ at $t=100\Delta t$ [see Fig. 10(a)]. Four parts of the curve are show: (1) on the left of the source, the wave remains in the scope of $(0,0.1)$, (2) in the region of wave motion, the wave still exists, (3) in the residue region, the wave remains within the scope of $(0,0.025)$, and (4) in the rest region, the residue errors are zero. In Fig. 10(b), we plot the curve of the residue errors $e=|\rho_D-\rho_I|$ versus X axis with a fixed $y=50\Delta y$ at $t=200\Delta t$. In this case, the residue errors reduce into the scope of $(0,0.005)$.

The curve of the recovery errors $R=|S_D-S_I|$ versus Y axis with a fixed $x=20\Delta x$ at $t=100\Delta t$ is given [see Fig. 11(a)]. We find that wave recovery errors are in the scope of $(0,0.04)$. In Fig. 11(b), we plot the curve of the recovery errors $R=|S_D-S_I|$ versus Y axis with a fixed $x=20\Delta x$ at

$t=200\Delta t$. At $t=200\Delta t$, the recovery errors are in the scope of $(0,0.04)$.

From Figs. 9–11, we find the lattice Boltzmann model possesses the reversibility in time in the sense of the small residue errors and small recovery errors.

E. Damped sound

In the small perturbation flows, the fluid medium is assumed to have an undisturbed state of rest, with uniform properties, density ρ_0 , pressure p_0 , and velocity $\mathbf{v}_0=0$. The acoustic motions produce deviations from the uniform state

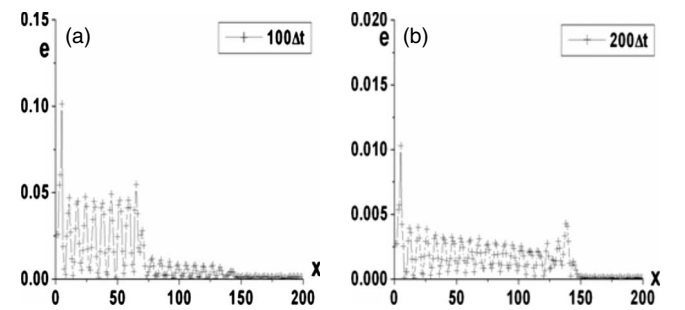


FIG. 10. (a) The curve of the residue errors $e=|\rho_D-\rho_I|$ versus X axis with a fixed $y=50\Delta y$ at $t=100\Delta t$. (b) The curve of the residue errors $e=|\rho_D-\rho_I|$ versus X axis with a fixed $y=50\Delta y$ at $t=200\Delta t$. The coordinates are denoted by the numbers of cells in x and y directions. Parameters are $c=3.0$, lattice size 200×100 , $\tau=0.5$, $n=1.0$, and $m=\frac{3}{16}$.

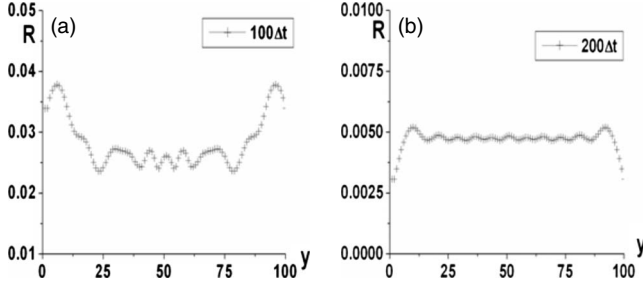


FIG. 11. (a) The curve of the recovery errors $R=|S_D-S_I|$ versus Y axis with a fixed $x=20\Delta x$ at $t=100\Delta t$. (b) The curve of the recovery errors $R=|S_D-S_I|$ versus Y axis with a fixed $x=20\Delta x$ at $t=200\Delta t$. The coordinates are denoted by the numbers of cells in x and y directions. Parameters are $c=3.0$, lattice size 200×100 , $\tau=0.5$, $n=1.0$, and $m=\frac{3}{16}$.

which are called small perturbations, thus the instantaneous local density ρ , pressure p , and velocity \mathbf{v} are given by

$$\rho = \rho_0 + \tilde{\rho}, \quad p = p_0 + \tilde{p}, \quad \mathbf{v} = \mathbf{v}_0 + \tilde{\mathbf{v}}, \quad (75)$$

where $\tilde{\rho}$, \tilde{p} , and $\tilde{\mathbf{v}}$ are the small perturbation in density, pressure, and velocity, respectively. According to the derivation for the conditions of the higher-order moments in Appendix, Eqs. (34) and (35) will be

$$\frac{\partial \tilde{\rho}}{\partial t} + \rho_0 \frac{\partial \tilde{u}_j}{\partial x_j} = O(\varepsilon^4), \quad (76)$$

$$\rho_0 \frac{\partial \tilde{u}_i}{\partial t} + c_s^2 \frac{\partial \rho \delta_{ij}}{\partial x_j} = -R_3 + O(\varepsilon^4). \quad (77)$$

In Eq. (77), R_3 is

$$R_3 = \varepsilon^3 C_4 (-\lambda^2 m^2 + 9\beta) \rho_0 \frac{\partial^3}{\partial x_i \partial x_j \partial x_k} \left(\frac{\partial}{\partial x_k} \tilde{u}_k \right). \quad (78)$$

Equations (76) and (77) are the sound propagation equations. The viscous damping term is $-R_3$.

In Ref. [2], the correct scaling is given. Based on the correct scaling expression, those scales are

$$x_j = \delta^{-1} x'_j, \quad t = \delta^{-1} t', \quad \tilde{\rho} = \delta^a \rho', \quad \tilde{u}_j = \delta^a u'_j, \quad (79)$$

where $a > 0$ and δ is a small parameter. x'_j , t' , ρ' , and u'_j are dimensionless spatial coordinate, time, density, and velocity, respectively. For the undamped sound waves, we assume that the sound wave equations are the scale δ^{a+1} , thus, we have $a > 0$. On the other hand, the viscous damping term is

$$R_3 = O(\delta^{a+4}) = O(\varepsilon^4). \quad (80)$$

Selecting $\delta = \varepsilon$, then we obtain $a > 0$. Therefore, density and velocity perturbations with amplitudes $o(1)$ on temporal and spatial scales $O(\delta)$ propagate as sound waves with speed c_s . The analyses are in full agreement with the results in the literature [2].

Let us consider a rectangle region $[0, 200\Delta x] \times [0, 100\Delta y]$, where $\Delta x = \Delta y = 0.01$. The line segment source is located at $x=5\Delta x$ from $y=0$ to $y=100\Delta y$ with source $\sin(\omega t)$. We plot the curve of the perturbation density $\tilde{\rho}$ ver-

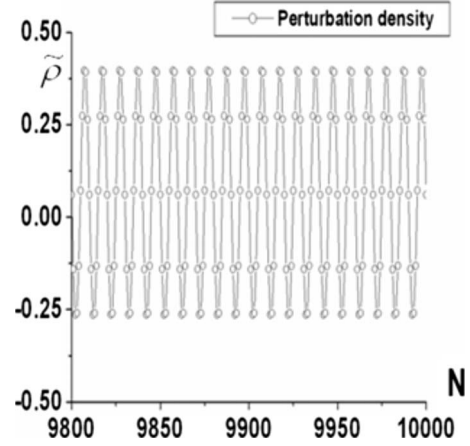


FIG. 12. The curve of the perturbation density $\tilde{\rho}$ versus time steps with a fixed $x=100\Delta x$, $y=50\Delta y$ from time steps $N=9800$ to $N=10\,000$. Parameters are $c=3.0$, lattice size 200×100 , $\tau=0.5$, $n=1.0$, and $m=\frac{3}{16}$.

sus time steps with a fixed $x=100\Delta x$, $y=50\Delta y$ from time steps $N=9800$ to $N=10\,000$ (see Fig. 12). The result shows that sound wave is undamped sound wave.

IV. CONCLUSION

In this paper, a lattice Boltzmann model with the third-order accuracy for wave propagation is proposed. In this model, we employ the higher-order moment method. The method is based on the solution of a series of partial differential equations obtained by using multiscale technique and Chapman-Enskog expansion. In order to obtain the lattice Boltzmann model for the wave equation with higher-order accuracy of truncation errors, we removed the second-order dissipation term and the third-order dispersion term by employing the moments up to fourth order. The reversibility in time appears owing to the absence of the second-order dissipation term and the third-order dispersion term. The sound wave and damped sound are discussed. In this model, the sound wave is undamped. Numerical examples show the interference, diffraction, and wave passing through a convex lens. On the other hand, the numerical results show that this model possesses the reversibility in time and without damp in propagation.

Though the intensity of wave is weakened as it passes through the holes of baffle plates, the optical phenomena can be observed clearly. It indicates that the model with such accuracy can be used to simulate wave propagation sufficiently.

The goal of the paper is to provide an effective numerical method for wave propagation and an idea of how to simulate light wave propagation. Perhaps, this feature can be demonstrated more strikingly by the Maxwell equations in electrodynamics. These are our future works.

ACKNOWLEDGMENTS

This work is Project 20092005 supported by Graduate Innovation Fund of Jilin University, the National Nature Sci-

ence Foundation of China (Grant No. 90305013), and the ChuangXin Foundation of Jilin University (No. 2004CX041). We would like to thank Dong Yinfeng, Liu Yanhong, Yan Bo, Wang Huimin, and Li Tingting for their many helpful suggestions.

APPENDIX

From Eq. (36), we have

$$E_1 = 0, \quad (\text{A1})$$

$$\begin{aligned} T_2 &= \frac{\partial E_1}{\partial t} - \frac{\partial R_1}{\partial x_i} = -\frac{\partial R_1}{\partial x_i} = -\frac{\partial}{\partial x_i} \varepsilon C_2 \frac{\partial}{\partial x_k} \left(\frac{\partial \pi_{ki}^0}{\partial t_0} + \frac{\partial P_{ijk}^0}{\partial x_j} \right) \\ &= -\varepsilon C_2 \frac{\partial}{\partial x_i} \frac{\partial}{\partial x_k} \left(\frac{\partial \lambda m \rho \delta_{ki}}{\partial t_0} + \frac{\partial P_{ijk}^0}{\partial x_j} \right) \\ &= -\varepsilon C_2 \frac{\partial}{\partial x_i} \frac{\partial}{\partial x_k} \left(-\lambda m \delta_{ki} \frac{\partial \rho u_j}{\partial x_j} + \frac{\partial P_{ijk}^0}{\partial x_j} \right). \end{aligned} \quad (\text{A2})$$

Substituting $P_{ijk}^0 = \frac{1}{3} \lambda m \rho (u_i \delta_{jk} + u_j \delta_{ik} + u_k \delta_{ij})$ into Eq. (A2), then

$$\begin{aligned} T_2 &= -\varepsilon C_2 \frac{\partial}{\partial x_i} \frac{\partial}{\partial x_k} \frac{\partial}{\partial x_j} (-\lambda m \delta_{ki} \rho u_j + P_{ijk}^0) \\ &= -\lambda m \varepsilon C_2 \frac{\partial}{\partial x_i} \frac{\partial}{\partial x_k} \frac{\partial}{\partial x_j} \left(-\frac{2}{3} \delta_{ki} \rho u_j + \frac{1}{3} \delta_{kj} \rho u_i + \frac{1}{3} \delta_{ij} \rho u_k \right) \\ &= -\lambda m \varepsilon C_2 \left[-\frac{2}{3} \frac{\partial}{\partial x_k} \frac{\partial}{\partial x_i} \frac{\partial}{\partial x_j} \rho u_j + \frac{1}{3} \frac{\partial}{\partial x_k} \frac{\partial}{\partial x_i} \frac{\partial}{\partial x_j} \rho u_i \right. \\ &\quad \left. + \frac{1}{3} \frac{\partial}{\partial x_i} \frac{\partial}{\partial x_j} \frac{\partial}{\partial x_k} \rho u_k \right] = 0. \end{aligned} \quad (\text{A3})$$

Equation (44) becomes

$$\begin{aligned} T_3 &= \frac{\partial E_2}{\partial t} - \frac{\partial R_2}{\partial x_i} = \frac{\partial E_2}{\partial t} - \frac{\partial}{\partial x_i} \\ &\quad \times \left[\varepsilon^2 \sum_{\alpha} m_{\alpha} \left(2C_2 \Delta \frac{\partial}{\partial t_1} f_{\alpha}^{(0)} + C_3 \Delta^3 f_{\alpha}^{(0)} \right) e_{\alpha i} \right] \\ &= \frac{\partial E_2}{\partial t} - \varepsilon^2 C_3 \frac{\partial}{\partial x_i} \sum_{\alpha} m_{\alpha} \Delta^3 f_{\alpha}^{(0)} e_{\alpha i}, \end{aligned} \quad (\text{A4})$$

where

$$\begin{aligned} E_2 &= \varepsilon^2 \sum_{\alpha} m_{\alpha} \left(C_3 \Delta^3 + 2C_2 \Delta \frac{\partial}{\partial t_1} \right) f_{\alpha}^{(0)} \\ &= \varepsilon^2 C_3 \sum_{\alpha} \left(\frac{\partial}{\partial t_0} + e_{\alpha j} \frac{\partial}{\partial x_j} \right)^3 f_{\alpha}^{(0)} m_{\alpha} \\ &= \varepsilon^2 C_3 \frac{\partial}{\partial t_0} \left[\frac{\partial}{\partial t_0} \left(\frac{\partial \rho}{\partial t_0} + \frac{\partial \rho u_j}{\partial x_j} \right) + \frac{\partial}{\partial x_m} \left(\frac{\partial \rho u_m}{\partial t_0} + \frac{\partial \pi_{jm}^0}{\partial x_j} \right) \right] \\ &\quad + \frac{\partial}{\partial x_k} \left[\frac{\partial}{\partial t_0} \left(\frac{\partial \rho u_k}{\partial t_0} + e_{\alpha j} \frac{\partial \pi_{kj}^0}{\partial x_j} \right) + \frac{\partial}{\partial x_m} \left(\frac{\partial \pi_{km}^0}{\partial t_0} + \frac{\partial P_{jkm}^0}{\partial x_j} \right) \right] \\ &= \varepsilon^2 C_3 \frac{\partial}{\partial x_k} \frac{\partial}{\partial x_m} \left(\frac{\partial \pi_{km}^0}{\partial t_0} + \frac{\partial P_{jkm}^0}{\partial x_j} \right) = 0, \end{aligned} \quad (\text{A5})$$

$$\begin{aligned} \sum_{\alpha} m_{\alpha} \Delta^3 f_{\alpha}^{(0)} e_{\alpha i} &= C_2 \sum_{\alpha} \left(\frac{\partial}{\partial t_0} + e_{\alpha j} \frac{\partial}{\partial x_j} \right)^3 f_{\alpha}^{(0)} m_{\alpha} e_{\alpha i} \\ &= \frac{\partial}{\partial t_0} \left[\frac{\partial}{\partial x_m} \left(\frac{\partial \pi_{im}^0}{\partial t_0} + \frac{\partial P_{ijm}^0}{\partial x_j} \right) \right] \\ &\quad + \frac{\partial}{\partial x_k} \left[\frac{\partial}{\partial t_0} \left(\frac{\partial \pi_{ik}^0}{\partial t_0} + e_{\alpha j} \frac{\partial P_{kij}^0}{\partial x_j} \right) \right. \\ &\quad \left. + \frac{\partial}{\partial x_m} \left(\frac{\partial P_{ikm}^0}{\partial t_0} + \frac{\partial Q_{ijkm}^0}{\partial x_j} \right) \right]. \end{aligned} \quad (\text{A6})$$

Substituting $Q_{ijkl}^0 = \frac{1}{3} \lambda^2 m^2 \rho (\delta_{ij} \delta_{kl} + \delta_{ik} \delta_{jl} + \delta_{il} \delta_{jk})$ into Eq. (A6), we have

$$\begin{aligned} T_3 &= -\varepsilon^2 C_3 \frac{\partial}{\partial x_i} \sum_{\alpha} m_{\alpha} \Delta^3 f_{\alpha}^{(0)} e_{\alpha i} = -\varepsilon^2 C_3 \frac{\partial}{\partial x_k} \frac{\partial}{\partial x_i} \frac{\partial}{\partial x_m} \\ &\quad \times \left[-\frac{1}{3} (\lambda m)^2 \frac{\partial \rho}{\partial x_j} (\delta_{jk} \delta_{im} + \delta_{jm} \delta_{ik} + \delta_{ij} \delta_{km}) + \frac{\partial Q_{ijkm}^0}{\partial x_j} \right] = 0. \end{aligned} \quad (\text{A7})$$

The error T_4 is

$$\begin{aligned} T_4 &= \frac{\partial E_3}{\partial t} - \frac{\partial R_3}{\partial x_i} = \frac{\partial}{\partial t} \left[\varepsilon^3 \sum_{\alpha} m_{\alpha} \left(C_4 \Delta^4 f_{\alpha}^{(0)} + C_2 \frac{\partial^2}{\partial t_1^2} f_{\alpha}^{(0)} \right) \right] \\ &\quad - \frac{\partial}{\partial x_i} \left[\varepsilon^3 \sum_{\alpha} m_{\alpha} \left(C_4 \Delta^4 f_{\alpha}^{(0)} + C_2 \frac{\partial^2}{\partial t_1^2} f_{\alpha}^{(0)} \right) e_{\alpha i} \right]. \end{aligned} \quad (\text{A8})$$

In Eq. (A8),

$$\sum_{\alpha} m_{\alpha} \Delta^4 f_{\alpha}^{(0)} = \frac{\partial}{\partial x_k} \frac{\partial}{\partial x_i} \frac{\partial}{\partial x_m} \left(\frac{\partial P_{ikm}^0}{\partial t_0} + \frac{\partial Q_{ijkm}^0}{\partial x_j} \right) = 0, \quad (\text{A9})$$

$$\begin{aligned} \sum_{\alpha} m_{\alpha} \frac{\partial^2}{\partial t_1^2} f_{\alpha}^{(0)} &= \frac{\partial}{\partial t_1} \frac{\partial}{\partial t_1} \sum_{\alpha} m_{\alpha} f_{\alpha}^{(0)} \\ &= \frac{\partial}{\partial t_1} \left(-C_2 \sum_{\alpha} m_{\alpha} \Delta^2 f_{\alpha}^{(0)} \right) = 0, \end{aligned} \quad (\text{A10})$$

$$\begin{aligned} \sum_{\alpha} m_{\alpha} \frac{\partial^2}{\partial t_1^2} f_{\alpha}^{(0)} e_{\alpha i} &= \frac{\partial}{\partial t_1} \frac{\partial}{\partial t_1} \sum_{\alpha} m_{\alpha} f_{\alpha}^{(0)} e_{\alpha i} \\ &= \frac{\partial}{\partial t_1} \left(-C_2 \sum_{\alpha} m_{\alpha} \Delta^2 f_{\alpha}^{(0)} e_{\alpha i} \right) = 0. \end{aligned} \quad (\text{A11})$$

Thus,

$$E_3 = 0, \quad (\text{A12})$$

$$T_4 = -\frac{\partial}{\partial x_i} \left[\varepsilon^3 \sum_{\alpha} m_{\alpha} C_4 \Delta^4 f_{\alpha}^{(0)} e_{\alpha i} \right] = -\varepsilon^3 C_4 \frac{\partial}{\partial x_i} \frac{\partial}{\partial x_k} \frac{\partial}{\partial x_m} \frac{\partial}{\partial x_j} \left(\frac{\partial Q_{ijkm}^0}{\partial t_0} + \frac{\partial R_{ijkml}^0}{\partial x_l} \right). \quad (\text{A13})$$

In Eq. (A13),

$$\frac{\partial Q_{ijkm}^0}{\partial t_0} = \frac{\partial}{\partial t_0} \left[\frac{1}{3} \lambda^2 m^2 \rho (\delta_{ij} \delta_{km} + \delta_{ik} \delta_{jm} + \delta_{im} \delta_{jk}) \right] = \frac{1}{3} \lambda^2 m^2 (\delta_{ij} \delta_{km} + \delta_{ik} \delta_{jm} + \delta_{im} \delta_{jk}) \left(-\frac{\partial \rho u_l}{\partial x_l} \right), \quad (\text{A14})$$

$$\begin{aligned} R_{ijkml}^0 &= \sum_{\alpha} m_{\alpha} f_{\alpha}^0 e_{\alpha i} e_{\alpha j} e_{\alpha k} e_{\alpha m} e_{\alpha l} = \sum_{\alpha} m (A_2 \rho e_{\alpha n} u_n e_{\alpha i} e_{\alpha j} e_{\alpha k} e_{\alpha m} e_{\alpha l} + B_2 \rho e_{\alpha n} u_n e_{\alpha i} e_{\alpha j} e_{\alpha k} e_{\alpha m} e_{\alpha l}) \\ &= m \frac{bc^6 \Delta_{ijkmln}}{D(D+2)(D+4)} \rho u_n (A_2 + 64B_2) = m \frac{bc^6 \Delta_{ijkmln}}{D(D+2)(D+4)} \rho u_n \frac{1}{12bc^4 m} [-48Dc^2 + 20D(D+2)\lambda m] \\ &= \frac{c^2 \Delta_{ijkmln}}{D(D+2)(D+4)} \rho u_n \frac{1}{12} [-48Dc^2 + 20D(D+2)\lambda m] = \frac{c^2 \Delta_{ijkmln}}{D(D+2)(D+4)} \rho u_n \left[-4Dc^2 + \frac{5}{3} D(D+2)\lambda m \right]. \end{aligned} \quad (\text{A15})$$

Therefore,

$$\begin{aligned} T_4 &= -\varepsilon^3 C_4 \frac{\partial}{\partial x_i} \frac{\partial}{\partial x_k} \frac{\partial}{\partial x_m} \frac{\partial}{\partial x_j} \left[\frac{1}{3} \lambda^2 m^2 (\delta_{ij} \delta_{km} + \delta_{ik} \delta_{jm} + \delta_{im} \delta_{jk}) \left(-\frac{\partial \rho u_l}{\partial x_l} \right) + \frac{\partial R_{ijkml}^0}{\partial x_l} \right] \\ &= -\varepsilon^3 C_4 \frac{\partial}{\partial x_i} \frac{\partial}{\partial x_k} \frac{\partial}{\partial x_m} \frac{\partial}{\partial x_j} \frac{\partial}{\partial x_l} \left[-\frac{1}{3} \lambda^2 m^2 \rho \Delta_{ijkml} u_l + 3\beta \rho (u_i \Delta_{jklm} + u_j \Delta_{iklm} + u_k \Delta_{jilm} + u_l \Delta_{jkim} + u_m \Delta_{jkli}) \right]. \end{aligned} \quad (\text{A16})$$

We have

$$T_4 = \frac{\partial E_3}{\partial t} - \frac{\partial R_3}{\partial x_i} = -\varepsilon^3 C_4 (-\lambda^2 m^2 + 9\beta) \nabla^4 (\nabla \cdot \rho \mathbf{u}), \quad (\text{A17})$$

where $\nabla^4 = \partial^4 / \partial x_i \partial x_i \partial x_k \partial x_k$ and $\beta = [c^2 / D(D+2)(D+4)] [-4Dc^2 + \frac{5}{3} D(D+2)\lambda m]$.

-
- [1] U. Frisch, B. Hasslacher, and Y. Pomeau, *Phys. Rev. Lett.* **56**, 1505 (1986).
[2] U. Frisch *et al.*, *Complex Syst.* **1**, 649 (1987).
[3] F. J. Higuera, S. Succi, and R. Benzi, *Europhys. Lett.* **9**, 345 (1989).
[4] Y. H. Qian, D. d'Humieres, and P. Lallemand, *Europhys. Lett.* **17**, 479 (1992).
[5] H. D. Chen, S. Y. Chen, and M. H. Matthaeus, *Phys. Rev. A* **45**, R5339 (1992).
[6] R. Benzi, S. Succi, and M. Vergassola, *Phys. Rep.* **222**, 145 (1992).
[7] S. Y. Chen and G. D. Doolen, *Annu. Rev. Fluid Mech.* **30**, 329 (1998).
[8] X. W. Shan and H. D. Chen, *Phys. Rev. E* **49**, 2941 (1994).
[9] M. Swift, W. Osborn, and J. Yeomans, *Phys. Rev. Lett.* **75**, 830 (1995).
[10] K. N. Premnath and J. Abraham, *J. Comput. Phys.* **224**, 539 (2007).
[11] A. K. Gunstensen, D. H. Rothman, S. Zaleski, and G. Zanetti, *Phys. Rev. A* **43**, 4320 (1991).
[12] D. J. Holdych, J. G. Georgiadis, and R. O. Buckius, *Phys. Fluids* **13**, 817 (2001).
[13] M. R. Swift *et al.*, *Phys. Rev. E* **54**, 5041 (1996).
[14] S. Succi, E. Foti, and F. J. Higuera, *Europhys. Lett.* **10**, 433 (1989).
[15] A. Ladd, *J. Fluid Mech.* **271**, 311 (1994).
[16] O. Filippova and D. Hanel, *Comput. Fluids* **26**, 697 (1997).
[17] X. F. Pan, A. G. Xu, G. C. Zhang, and S. Jiang, *Int. J. Mod. Phys. C* **18**, 1747 (2007).
[18] F. L. Hinton, M. N. Roseblush, S. K. Wang, Y. R. Lin-Liu, and R. L. Miller, *Phys. Rev. E* **63**, 061212 (2001).
[19] T. Kataoka and M. Tsutahara, *Phys. Rev. E* **69**, 056702 (2004).
[20] M. Bernaschi, S. Succi, and H. Chen, *J. Sci. Comput.* **16**, 135 (2001).
[21] Z. L. Guo, T. S. Zhao, and Y. Shi, *Phys. Rev. E* **70**, 066706 (2004).
[22] A. C. Velivelli and K. M. Bryden, *Physica A* **362**, 139 (2006).
[23] Y. L. Duan and R. X. Liu, *Comput. Appl. Math.* **206**, 432 (2007).
[24] G. W. Yan and J. Y. Zhang, *Math. Comput. Simul.* **79**, 1554 (2009).
[25] G. W. Yan and L. Yuan, *Physica D* **154**, 43 (2001).
[26] S. Succi, *Physica D* **69**, 327 (1993).
[27] S. Succi, *Comput. Phys. Commun.* **146**, 317 (2002).
[28] S. Palpacelli and S. Succi, *Phys. Rev. E* **75**, 066704 (2007).
[29] L. H. Zhong, S. D. Feng, P. Dong, and S. T. Gao, *Phys. Rev. E* **74**, 036704 (2006).
[30] Z. H. Chai and B. C. Shi, *Appl. Math. Model.* **32**, 2050 (2008).
[31] M. R. Wang, J. K. Wang, and S. Y. Chen, *J. Comput. Phys.*

- 226**, 836 (2007).
- [32] H. D. Chen, S. Y. Chen, G. Doolen, and Y. C. Lee, *Complex Syst.* **2**, 259 (1988).
- [33] C. Vanneste, P. Sebbah, and D. Sommette, *Europhys. Lett.* **17**, 715 (1992).
- [34] J. Buick, W. Easson, and C. Greated, *Int. J. Numer. Methods Fluids* **26**, 657 (1998).
- [35] P. J. McKerrow, S. M. Zhu, and S. New, *IEEE Trans. Rob. Autom.* **17**, 202 (2001).
- [36] B. James *et al.*, International Conference on Supercomputing Proceedings of the Seventh International Conference on Supercomputing, Tokyo, Japan, 1993 (unpublished), pp. 348–356.
- [37] D. Rothmann, *Geophys. Res. Lett.* **14**, 17 (1987).
- [38] J. I. Huang, Y. H. Chu, and C. S. Yin, *Geophys. Res. Lett.* **15**, 1239 (1988).
- [39] L. J. Huang and P. Mora, *Geophys. J. Int.* **119**, 766 (1994).
- [40] B. Chopard and P. O. Luthi, *Theor. Comput. Sci.* **217**, 115 (1999).
- [41] G. W. Yan, *J. Comput. Phys.* **161**, 61 (2000).
- [42] Y. W. Kwon and S. Hosoglu, *Comput. Struct.* **86**, 663 (2008).
- [43] W. S. Jiaung and J. R. Ho, *Phys. Rev. E* **77**, 066710 (2008).
- [44] J. M. Buick and J. A. Cosgrove, *J. Phys. A* **39**, 13807 (2006).
- [45] P. J. Dellar, *Phys. Rev. E* **65**, 036309 (2002).
- [46] H. Y. Li and H. Ki, *Phys. Rev. E* **76**, 066707 (2007).
- [47] J. M. Buick, J. A. Cosgrove, and C. A. Greated, *Appl. Math. Model.* **28**, 183 (2004).
- [48] P. Mora, *J. Stat. Phys.* **68**, 591 (1992).
- [49] J. M. Buick, *Phys. Rev. E* **76**, 036713 (2007).
- [50] F. Qiu, F. Xu, Z. Fan, and N. Neophytos, *IEEE Trans. Vis. Comput. Graph.* **13**, 1576 (2007).
- [51] Y. Zhao *et al.*, *IEEE Trans. Vis. Comput. Graph.* **13**, 179 (2007).
- [52] Tosiya Taniuti and Katsunobu Nishihara, *Nonlinear Waves* (Pitman, Boston, 1983).
- [53] G. B. Whitham, *Linear and Nonlinear Waves* (Wiley, New York, 1974).
- [54] S. Chapman and T. G. Cowling, *The Mathematical Theory of Non-Uniform Gas* (Cambridge University Press, Cambridge, 1970).
- [55] D. Holdych *et al.*, *J. Comput. Phys.* **193**, 595 (2004).
- [56] C. W. Hirt, *J. Comput. Phys.* **2**, 339 (1968).
- [57] J. Wang and R. X. Liu, *J. Comput. Appl. Math.* **134**, 59 (2001).
- [58] G. Fairweather and A. R. Mitchell, *SIAM (Soc. Ind. Appl. Math.) J. Numer. Anal.* **4**, 163 (1967).
- [59] D. Halliday and R. Resnick, *Physics*, 3rd edition (Wiley, New York, 1978), Pt. II.